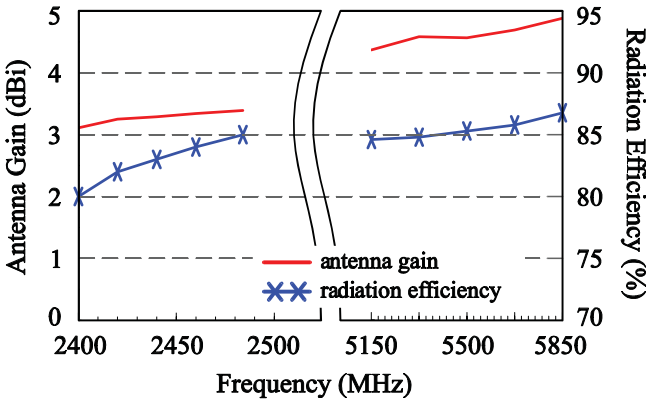

Figure 7 Measured antenna gain and simulated radiation efficiency for the WLAN band studied in Figure 2. [Color figure can be viewed in the online issue, which is available at www.interscience.wiley.com]

phone capable of UMTS/WLAN dual-mode operation, has been proposed. The proposed antenna can easily be fabricated by using a single metal plate, thus making it easy to construct at a low cost. Prototypes of the proposed antenna have been constructed and studied. A wide bandwidth of about 5 GHz (1818–6746 MHz) has been achieved, which makes the antenna very promising for covering the UMTS and the 2.4/5.2/5.8-GHz bands for UMTS/WLAN dual-mode operation. The experimental results also indicate that good radiation characteristics over the UMTS and WLAN bands have been obtained.

REFERENCES

1. M. Hammoud, P. Poey, and F. Colombel, Matching the input impedance of a broadband disc monopole, Electron Lett 29 (1993), 406-407.
2. N.P. Agrawall, G. Kumar, and K.P. Ray, Wide-band planar monopole antennas, IEEE Trans Antennas Propag 46 (1998), 294-295.
3. K.L. Wong, T.C. Tseng, and P.L. Teng, Low-profile ultra-wideband metal-plate antenna for mobile phone applications, Microwave Opt Technol Lett 43 (2004), 7-9.
4. S.Y. Lin, Multiband folded planar monopole antenna for mobile handset, IEEE Trans Antennas Propag 52 (2004), 1790-1794.
5. Y.T. Liu, Wideband stubby monopole antenna for mobile phone, Electron Lett 42 (2006), 385-387.
6. Y.T. Liu, A stubby monopole antenna for UMTS mobile phones with E911 function, Microwave Opt Technol Lett 49 (2007), 380-382.
7. K.L. Wong, Planar antennas for wireless communications, Wiley, New York, 2003.
8. E. Antonino-Daviu, M. Cabedo-Fabres, M. Ferrando-Bataller, and A. Valero-Nogueira, Wideband double-fed planar monopole antennas, Electron Lett 39 (2003), 1635-1636.
9. Ansoft Corporation, HFSS, http://www.ansoft.com/products/hfss/.

ENHANCEMENT OF BROADBAND PERFORMANCE FOR ON-CHIP SPIRAL INDUCTORS WITH INNER-PATTERNED-GROUND

Jinglin Shi,[1] Sheng Sun,[2] Yong Zhong Xiong,[1] Wooi Gan Yeoh,[1] and Kiat Seng Yeo[2]
[1] Institute of Microelectronics, Singapore 117685; Corresponding author: jinglin@ime.a-star.edu.sg
[2] Nanyang Technology University, Singapore 639798

Received 23 November 2007

ABSTRACT: *A set of on-chip spiral inductors with novel inner-patterned-ground (IPG) is presented in this article to enhance the broadband performance. By grounding the simple center metal cross, the IPG structure, an additional inner ground path is formed, the input impedance of the spiral inductor is reduced at the higher frequency range. When compared with conventional inductors, the quality factor (Q) of the IPG inductors increases by 15–30% over the frequency range of 15–35 GHz. The IPG inductors can be modeled based on a simple lumped equivalent circuit. The extracted inductance and quality factors are verified by on-wafer measurement up to 50 GHz.* © 2008 Wiley Periodicals, Inc. Microwave Opt Technol Lett 50: 1744–1746, 2008; Published online in Wiley InterScience (www.interscience.wiley.com). DOI 10.1002/mop.23545

Key words: *on-chip spiral inductor; CMOS; inner-patterned-ground; quality factor*

1. INTRODUCTION

Silicon on-chip spiral inductors have been widely used in radio frequency integrated circuits (RFICs) for wireless communication systems such as wireless local area networks, personal handsets, and global positioning systems. Monolithic inductors have drawn tremendous research effort over the past decades, especially in recent years. A lot of modeling approaches have been reported in recent years [1-3]. But only a few works has been done on the novel design of the spiral inductor structure itself [4-6].

The FCC has opened up 22–29 GHz for ultrawideband vehicle radar systems [7]. Consequently, a lot of research work published on 24-GHz range, 24 GHz blocks, or transceivers [8, 9]. In this article, a novel inner-patterned-ground (IPG) structure is proposed for the design of broadband spiral inductors. The enhancement of quality factor over the frequency range of 15–35 GHz has been achieved as compared to the conventional inductors. The resultant performance is verified by measurement based on standard 0.18 μm CMOS technology.

2. INDUCTOR DESIGN

A set of inductors with and without IPG structure is fabricated using standard 0.18 μm CMOS technology (substrate resistivity 10 O-cm). Figures 1(a) and 1(b) show the die photo of the conventional spiral inductor and the IPG inductor, respectively, fabricated using standard CMOS process technology with six layers of metal TiW/Al-1% Si/TiW interconnects. The inductors have an inner diameter of 40 μm and 50 μm, a metal winding width of 5 μm, a metal winding spacing of 5 μm and two turns. The IPG inductor has a metal cross, i.e., the IPG structure inside the inductor coil which consists of metal 1 to metal 6 together with vials. The width of the cross bar is 3 μm, and the distance from the edge of the sign to the inductor inner edge is 5 μm. The cross sign is connected to the ground bar through metal 1.

Because of the implementation of the IPG structure, the magnetic field and the electric field to the substrate are modified. At

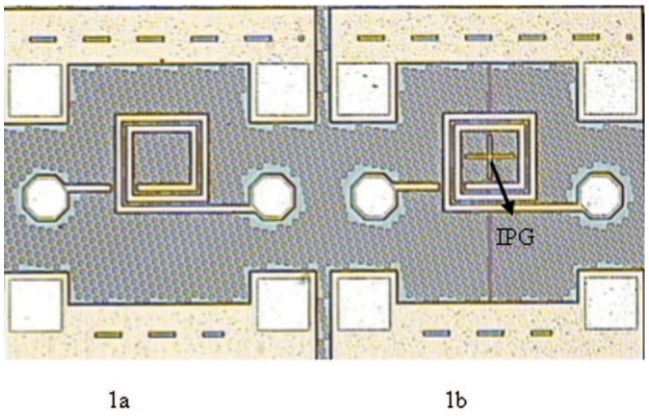

Figure 1 Die photos of the conventional and novel inductor (a, conventional; b, inductor with IPG). [Color figure can be viewed in the online issue, which is available at www.interscience.wiley.com]

low-frequency, the performances of the two sets of inductors are the same. As frequency increases, the electric field to the silicon substrate is partially changed to the IPG.

Figure 2 shows the equivalent circuit for the inductors. The dash box refers to the equivalent circuits of the conventional inductor based on the concept as in [10], where R_2 and L_2 account for high-frequency effect. The port 1 to port 2 coupling capacitance is omitted due to the calculated value is less than 1 f using the method descried in [11]. The IPG provides one additional path to ground which is modeled by series C_3, R_3, and L_3. For simplicity and clarity, we use _CON and _IPG for type 1a inductor in Figure 1(a) and type 1b inductor in Figure 1(b) through this article.

3. EXPERIMENTAL RESULTS AND DISCUSSIONS

The fabricated structures were measured using an HP8510C network analyzer, a Cascade probe station, and Cascade infinity GSG probes from 100 MHz to 50.1 GHz and de-embedded with the open structure. The inductance and quality factor are calculated by Eqs. (1) and (2) with the Y-parameters converted from measured de-embedded S-parameters

$$L = \frac{\mathrm{Im}(1/Y_{11})}{\omega} \tag{1}$$

$$Q = \frac{\mathrm{Im}(1/Y_{11})}{\mathrm{Re}(1/Y_{11})} \tag{2}$$

Figure 3 shows the extracted inductance values for these inductors.

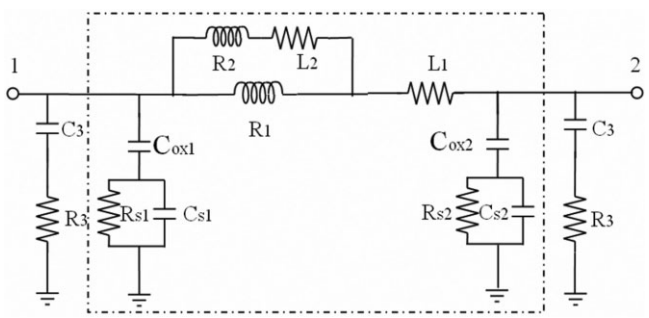

Figure 2 Equivalent circuits of the conventional and IPG inductors (dash line box is a simplified circuit model for the conventional inductor)

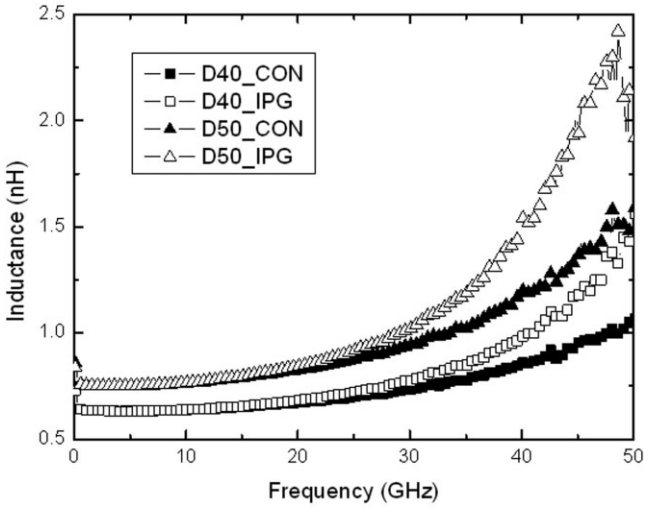

Figure 3 Extracted inductance of the two sets inductors with inner diameters of 40 μm and 50 μm. Legend: ■ D40_CON, □ D40_IPG, ▲ D50_CON, △ D50_IPG

The inductance of the novel inductor with IPG increases faster than that of the conventional inductor as the frequency goes up.

Figure 4 shows the extracted quality factors of these inductors. The quality factors (Q) increase to 15–30% from 20–35 GHz. It increases more for the 50 μm diameter inductor than the 40 μm diameter inductor. From these figures, we can conclude the IPG has effect on both the inductance and quality factor at higher frequency range. The equivalent circuit values of the conventional and novel inductors are tabulated in Tables 1 and 2, respectively. In Table 2, R_1, L_1, R_2, and L_2 are omitted because they are the same as in Table 1.

Figure 5 shows the extracted inductance and quality factor from the circuit model (_C) and measurement data (_M) for the 50 μm inductor. The circuit simulation data show good agreement with the measurement data.

Figure 6 shows the input impedance of the inductors. The impedance of the novel inductor is flatter than that of the conventional inductor at higher frequency range which further confirms that IPG improves the inductor performance.

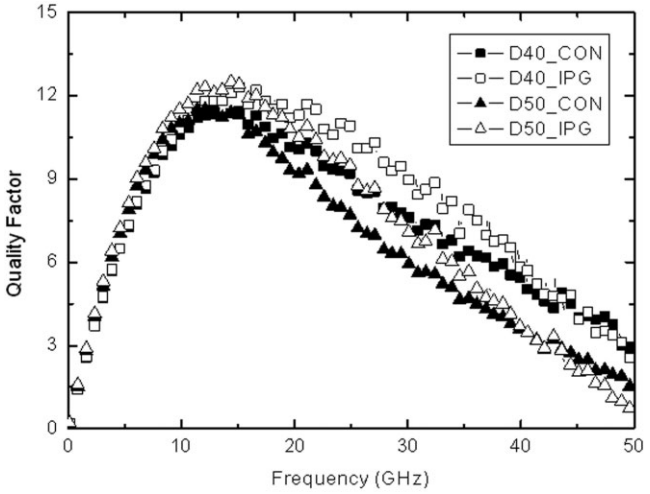

Figure 4 Extracted quality factor of the two sets inductors with inner diameters of 40 μm and 50 μm. Legend: ■ D40_CON, □ D40_IPG, ▲ D50_CON, △ D50_IPG

TABLE 1 Equivalent Circuit Values for Conventional Inductors

Ind_con	R_1 (Ω)	L_1 (pH)	R_2 (Ω)	L_2 (pH)	C_{ox1} (fF)	C_{S1} (fF)	R_{S1} (Ω)	C_{ox2} (fF)	C_{S2} (fF)	R_{S2} (Ω)
D40	4.4	580	3	80	13	1	280	14	2	250
D50	5.6	690	3.2	80	14.2	2	220	15	2.5	200

TABLE 2 Equivalent Circuit Values for Inductors with IPG

Ind_nov	C_{ox1} (fF)	C_{S1} (fF)	R_{S1} (Ω)	C_{ox2} (fF)	C_{S2} (fF)	R_{S2} (Ω)	C_3 (fF)	R_3 (Ω)	L_3 (pH)
D40	11	10	130	13	10	100	3	2.5	10
D50	12	10	110	14	10	95	3	2.5	10

4. CONCLUSION

In this article, novel spiral inductors with IPG were designed, fabricated, and characterized experimentally. The improvement of the quality factor is obvious and it would benefit broadband applications without any extra cost.

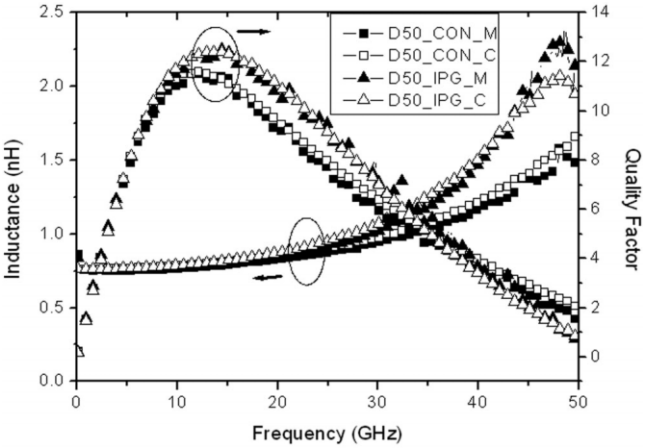

Figure 5 Comparison of inductance and quality factor of measured and modeled the inductor with inner diameter 50 μm. Legend: ■ D50_CON_M, □ D50_CON_C, ▲ D50_IPG_M, △ D50_IPG_C

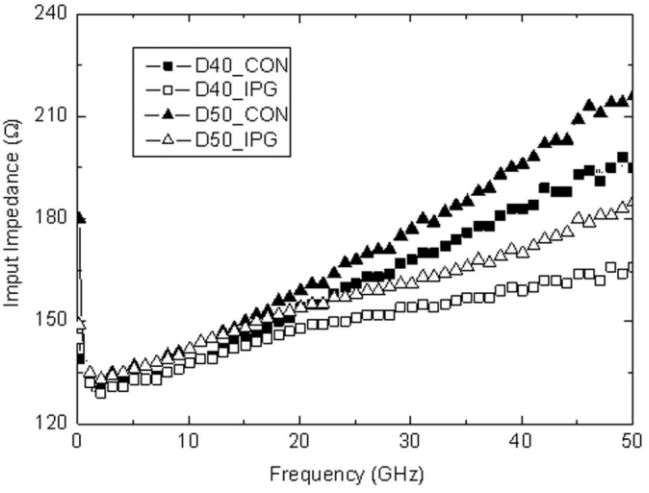

Figure 6 Comparison of input impedances of the conventional and IPG inductors with inner diameter of 40 μm and 50 μm. Legend: ■ D40_CON, □ D40_IPG, ▲ D50_CON, △ D50_IPG

REFERENCES

1. S. Jenei, B.K.J.C. Nauwelaers, and S. Decoutere, Physics-based closed-form inductance expression for compact modeling of integrated spiral inductors, IEEE J Solid-State Circuits 37 (2002), 77–80.
2. A.C. Watson, D. Melendy, P. Francis, K. Hwang, and A. Weisshaar, A comprehensive compact-modeling methodology for spiral inductors in silicon-based RFICs, IEEE Trans Microwave Theory Tech 52 (2004), 849–857.
3. F. Huang, N. Jiang, and E. Bian, Characteristic-function approach to parameter extraction for asymmetric equivalent circuit of on-chip spiral inductors, IEEE Trans Microwave Theory Tech 54 (2006), 115–119.
4. Y.-Y. Wang and Z.-F. Li, Group-cross symmetrical inductor (GCSI): a new inductor structure with higher self-resonance frequency and Q factors, IEEE Trans Mag 42 (2006), 1325–1330.
5. H. Gau, S. Sang, R.-T. Wu, F.-J. Shen, H.-H. Chen, A. Chen, and J. Ko, Novel fully symmetrical inductor, IEEE Electron Device Lett 25 (2004), 608–609.
6. M.D. Philips and R.K. Settaluri, A novel toroidal inductor structure with through-hole vias in ground plane, IEEE Trans Microwave Theory Tech 54 (2006), 1325–1330.
7. Code of federal regulations, title 47-telecommunication, Chapter I, Federal Commun. Commission, pt. 15-Radio FrequencyDevices, secs. 15.515 and 15.521, 2004.
8. I. Gresham, A. Jenkins, R. Egri, C. Eswarappa, F. Kolak, R. Wohlert, J. Bennett, and J. Lanteri, Ultra wide band 24 GHz automotive radar front-end, in IEEE MTT-S International Microwave Symposium Digest, June, 2003, pp. 369–372.
9. H. Hashemi, X. Guan, A. Komijani, and A. Hajimiri, A 24-GHz SiGe phased-array receiver-LO phase-shifting approach, IEEE Trans Microwave Theory Tech 53 (2005), 614–626.
10. L.F. Tiemeijer, R.J. Havens, Y. Bouttement, and H.J. Pranger, Physical-based wideband predictive compact model for inductors with high amounts of dummy metal fill, IEEE Trans Microwave Theory Tech 54 (2006), 3378–3386.
11. C.-Y. Lee, T.-S. Chen, J.D.-S. Deng, and C.-H. Kao, A simple systematic spiral inductor design with perfected Q improvement for CMOS application, IEEE Trans Microwave Theory Tech 53 (2005), 523–528.